Virology 526 (2019) 173–179

Contents lists available at ScienceDirect

Virology

journal homepage: www.elsevier.com/locate/virology

Vascular permeability in the brain is a late pathogenic event during Rift Valley fever virus encephalitis in rats

Aaron W. Walters[a,b,1], Michael R. Kujawa[a,b,1], Joseph R. Albe[a,b], Douglas S. Reed[a,c], William B. Klimstra[a,c], Amy L. Hartman[a,b,*]

[a] Center for Vaccine Research, University of Pittsburgh, Pittsburgh, PA, USA
[b] University of Pittsburgh Graduate School of Public Health, Pittsburgh, PA, USA
[c] Department of Immunology, University of Pittsburgh School of Medicine, Pittsburgh, PA, USA

ARTICLE INFO

Keywords:
Rift valley fever
Viral encephalitis
Blood brain barrier
Aerosol infection

ABSTRACT

Rift Valley fever virus (RVFV) is a zoonotic disease of livestock that causes several clinical outcomes in people including febrile disease, hemorrhagic fever, and/or encephalitis. After aerosol infection with RVFV, Lewis rats develop lethal encephalitic disease, and we use this as a model for studying disease mechanisms of RVFV infection in the brain. Permeability of the brain vasculature in relation to virus invasion and replication is not known. Here, we found that vascular permeability in the brain occurred late in the course of infection and corresponded temporally to expression of matrix metalloproteinase-9 (MMP-9). Virus replication was ongoing within the central nervous system for several days prior to detectable vascular leakage. Based on this study, vascular permeability was not required for entry of RVFV into the brain of rats. Prevention of vascular leakage late in infection may be an important component for prevention of lethal neurological disease in the rat model.

1. Introduction

Understanding the pathogenesis of neurological disorders caused by arboviruses is fundamental to the rational design of therapeutics to treat viral encephalitis. Rift Valley fever virus (RVFV; family *Phenuiviridae,* formerly *Bunyaviridae*) infection of people is typically a self-limiting febrile illness yet can progress to vision problems, hepatic disease with hemorrhagic fever, and neurological complications (Al-Hazmi et al., 2003; Boushab et al., 2016; Mohamed et al., 2010; Rakotoarivelo et al., 2011). Neurological disease such as meningoencephalitis caused by RVFV leads to morbidity and mortality in people during human outbreaks and may pose a challenge for development of effective vaccines and therapeutics (Bird et al., 2012; Scharton et al., 2014). While RVF is a mosquito-transmitted disease, herdsmen, farmers, and other people living in close proximity to livestock or consuming animal products are at increased risk for infection and development of severe forms of RVF disease (Mutua et al., 2017; Nicholas et al., 2014). For individuals handling sick and dying animals, mucosal exposure of the eyes/nose/mouth or inhalation of virus from infected tissues may occur (Anyangu et al., 2010; Madani et al., 2003; Mutua et al., 2017). Intranasal or aerosol exposure to RVFV are both more likely to result in encephalitis in lab animals than subcutaneous injection (Bales et al., 2012; Dodd et al., 2014; Gowen et al., 2013; Hartman et al., 2014; Reed et al., 2013; Smith et al., 2012). After intranasal or inhalational exposure to wild-type RVFV, Lewis rats develop encephalitic disease with neurological signs (Bales et al., 2012; Caroline et al., 2016). Lewis rats represent a reproducible tractable model for understanding the pathogenic process leading to encephalitis in rats. We recently showed that disease in rats is accompanied by changes in the central nervous system (CNS) that encompass high levels of virus replication, infiltration of immune cells, and expression of inflammatory cytokines (Caroline et al., 2016). An unanswered question regarding RVFV infection of the CNS in the rat model is the timing of the permeability of the brain vasculature in relation to other pathogenic events.

Control of the vascular integrity of the CNS is mediated by the blood brain barrier (BBB), a reinforced endothelial cell layer designed to selectively limit exposure of the brain to toxins, pathogens, and other deleterious compounds. Endothelial cells within this barrier are reinforced by tight junctions (TJ) and are physically supported by surrounding astrocytes and pericytes. The ability of the BBB to keep viruses out of the brain is not absolute, and viruses have found ways to skirt the BBB by hematogenous (free virus passes from the blood directly through the BBB), neural (*via* infection of a peripheral neuron), or

* Corresponding author at: Center for Vaccine Research, University of Pittsburgh, Pittsburgh, PA, USA.
E-mail address: hartman2@pitt.edu (A.L. Hartman).
[1] These authors contributed equally to this work.

https://doi.org/10.1016/j.virol.2018.10.021
Received 9 August 2018; Received in revised form 8 October 2018; Accepted 19 October 2018
Available online 02 November 2018
0042-6822/

"Trojan horse" (virus hides in infected immune cells to enter the CNS) mechanisms (McGavern and Kang, 2011). Some pathogens use more than one mechanism, depending upon infection route or stage of disease progression (Cain et al., 2017; Schafer et al., 2011). Recent discovery of lymphatic vessels that drain the meninges presents a new potential avenue for CNS access by viruses (Louveau et al., 2015).

We report here our efforts to determine the temporal spread of virus throughout regions of the brain and compare this to when permeability of the brain vasculature occurs. We found that virus replication in the brain occurred prior to vascular permeability, which we detected 5 days after infection during a 7 day time course. Expression of MMP-9 occurred concomitant with vascular leakage. This work helps to further the understanding of the pathogenic events that occur in the rat model of RVF encephalitis.

2. Materials and methods

2.1. Biosafety and ethics

All experiments with live ZH501 Rift Valley Fever Virus were conducted in the Regional Biosafety Laboratory (RBL) at the University of Pittsburgh following the safety procedures described previously (Bales et al., 2012). The RBL is a registered BSL-3/ABSL-3 laboratory space with the CDC and USDA. Samples inactivated using the described methods were approved by a University of Pittsburgh biosafety oversight committee. All animal work conducted was reviewed and approved by the University of Pittsburgh IACUC.

2.2. Virus and cells

The ZH501 strain of Rift Valley Fever Virus used in these experiments was generously provided by Barry Miller (CDC, Fort Collins, Colorado) and Stuart Nichol (CDC, Atlanta, Georgia). The virus was generated by reverse-genetics based on the sequence of an isolate collected from a human patient during the 1977 Egyptian RVFV outbreak (ZH501 strain) (Meegan, 1979). The virus was then grown in Vero E6 cells using standard propagation procedures.

2.3. Animal experiments

Female Lewis rats (LEW/SsNHsd) were obtained from Harlan Laboratories between 8 and 10 weeks of age. RVFV ZH501 infections *via* aerosol were performed in a class III aerobiology cabinet as described previously (Bales et al., 2012). Rats were serially euthanized (3/day) though 6 dpi. Blood was drawn by cardiac puncture and saved for serum isolation. Rats were then perfused with PBS prior to organ collection. Virus was measured using q-RT-PCR as previously described (Caroline et al., 2016) and results are normalized to pfu and are expressed as pfu/ml equivalents. For measurement of MMP-9 quantification, the Rat Total MMP-9 Quantikine or DuoSet ELISA kits were used (R&D Systems; Cat. RMP900 and DY8174-05). Samples were homogenized and centrifuged to collect 200uL of supernatant for testing. Plates were read using the FLUOstar Omega (BMG Lab Tech). Calculations were performed using the Omega software. Reported values are in ng/ml, as indicated.

2.4. Measurement of vascular integrity

Lewis rats were infected by aerosol, and groups of three were sacrificed daily. Before euthanasia, fluorescein sodium salt (376 g/mol m.w.; 20 mg/rat; Sigma Aldrich) was injected *via* tail vein and given two minutes to circulate. Blood was drawn by cardiac puncture followed by perfusion with PBS. The fluorescein content from the serum and brain of each animal was extracted by TCA precipitation and fluorescent intensity was measured using FLUOstar Omega (BMG Lab Tech) as described previously (Cain et al., 2017). Fluorescence in each brain region was normalized against the serum to account for any variability in fluorescein salt injection that may have occurred.

For *in vivo* imaging, Lewis rats were infected by aerosol and monitored until 4–5 days post infection. At the time points indicated, Superhance 680 (Perkin Elmer; 1540 g/mol m.w.) was injected *via* the tail vein (9.1 nmole/rat). Infected rats were paired with an uninfected control animal, and each pair was imaged before Superhance 680 injection, 5 min, 3 h, 24 h, and 48 h after injection. All imaging was done using the Spectrum CT *In Vivo* Imaging System (IVIS; Perkin Elmer) in the BSL-3 lab. The brains were removed after euthanasia and imaged *ex vivo*. Reagent intensity was measured using Living Image Software (Perkin Elmer) after acquisition.

2.5. Statistics

Statistical analyses (*t*-tests, linear regression, Pearson's correlation) were performed using GraphPad Prism software (La Jolla, CA). Asterisks above symbols indicate statistical significance ($^{*}p < 0.05$ $^{**}p < 0.01$ $^{***}p < 0.001$ $^{****}p < 0.0001$).

3. Results

3.1. Temporal spread of RVFV through the brain

The Lewis rat model is useful for deciphering the *in vivo* pathogenic mechanisms of encephalitis caused by infection with RVFV (Bales et al., 2012; Caroline et al., 2016). After exposure to small particle aerosols containing the pathogenic wild-type ZH501 strain of RVFV, Lewis rats develop disease and succumb within 6–7 days (LD_{50} =112 pfu) (Bales et al., 2012). Rats appear clinically normal through 5 days post-infection (dpi). Signs of illness occur from 5 to 7 dpi include mild weight loss, fever, porphyrin staining, and neurological signs (head tremors and circling or rolling in the cage). Our previous work has defined physiological events that occur during the clinical window including granulocytosis, thrombocytopenia, pathological changes in CNS tissue (encephalitis, meningitis, and vasculitis), and chemokine expression in the brain (MCP-1, MCSF, Gro/KC, RANTES, IL-1β) (Bales et al., 2012; Caroline et al., 2016).

When rats were exposed to 1×10^3 pfu by aerosol, virus was first detectable in the cervical lymph nodes (CLN) and salivary glands at 1 dpi, followed by the olfactory bulb, cortex, liver, and spleen on 2 dpi (Fig. 1A,B). Viremia is not detectable until 3 dpi and remains low thereafter. CLN, spleen, and liver viral levels plateau at 3 dpi and remains at low levels for the duration. Conversely, viral titers in the brain rise rapidly and reach levels of up to 10^6 pfu/g tissue during the clinical window (gray shaded bars in Fig. 1). Virus spreads in an anterior–posterior direction, with virus appearing earliest and at highest levels in the olfactory bulb and latest and at lowest levels in the brain stem and spinal cord.

3.2. Vascular permeability in the brain is a late event during lethal infection

The integrity of the blood brain barrier is important to keep infectious agents and damaging compounds out of the brain and to maintain overall health of the CNS. During encephalitic viral infections, the loss of integrity of the BBB may allow a virus access to the brain or may be the result of pathogenic viral replication in the brain. The timing of brain vascular integrity during RVF encephalitis is unknown and is important for fully understanding the pathogenesis of RVF disease.

To address the timing of vascular permeability in relation to virus replication in the brain within RVFV-infected rats, we used two methods to measure the vascular integrity during the course of viral infection. Fluorescein (FITC) sodium salt has been used as an indicator of BBB permeability during arboviral infections (Cain et al., 2017). Due to its small mass (m.w. of 376), FITC-salt can identify small vascular

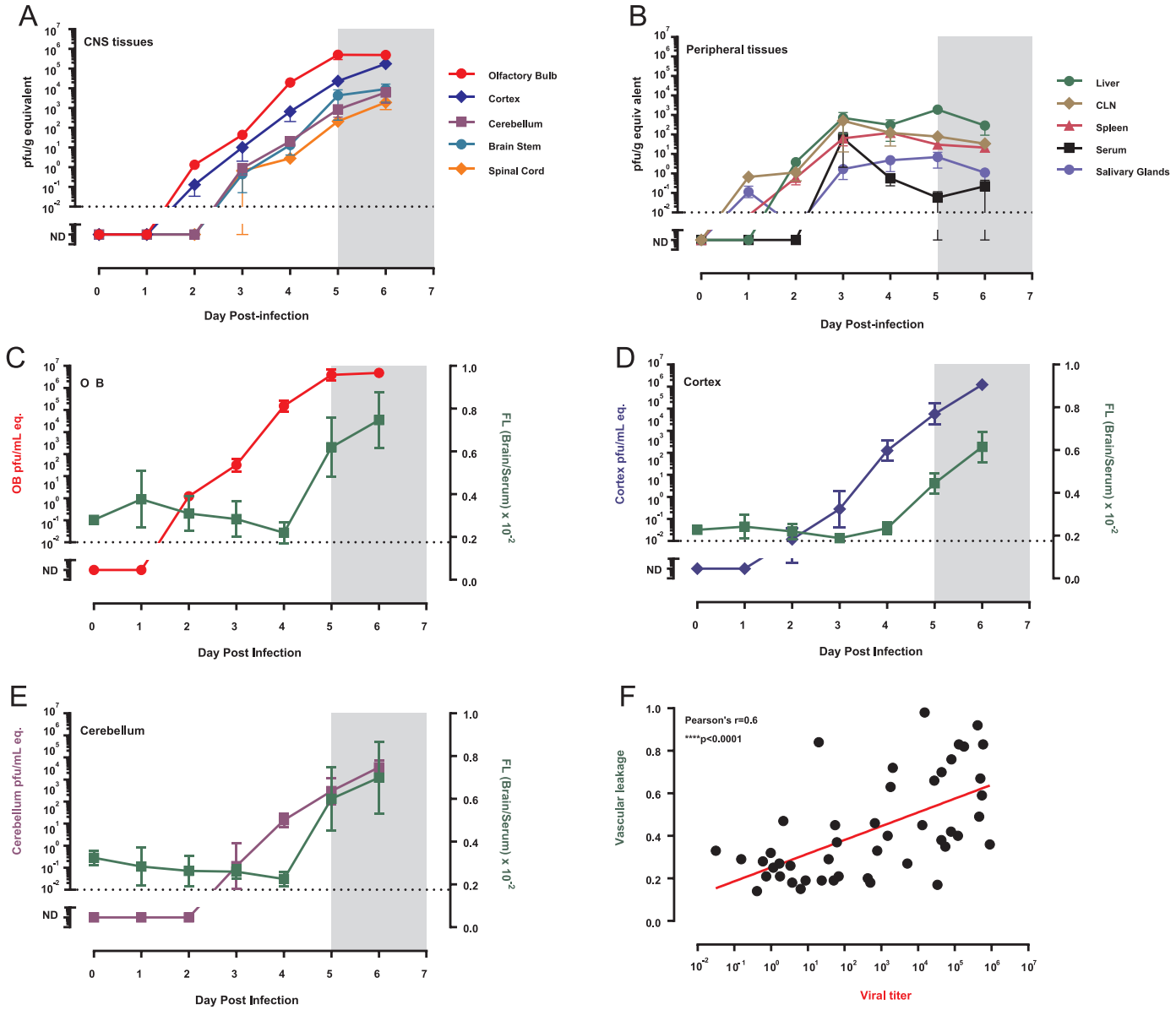

Fig. 1. Virus replication and vascular leakage during RVF encephalitis. Lewis rats were infected with 1×10^3 pfu of RVFV by aerosol and then serially euthanized (n = 3) over a time course of six days. (A-B) Virus levels in tissues and serum were measured by q-RT-PCR and compared to virus stock of known titer to generate pfu/g or pfu/ml equivalent (y-axes). (A) CNS tissues; (B) peripheral tissues. CLN = cervical lymph nodes. (C-E) Fluorescein-salt penetration of brain regions was normalized to serum (right y-axis; green). Corresponding viral q-RT-PCR results for each sample are normalized to plaque forming units and are represented as pfu/g equivalents (left y-axis). The limit of detection of the PCR assay is indicted by the horizontal dotted line. ND = below the limit of detection. The gray shaded area between 5 and 7 dpi represents the clinical window when rats display clinical signs of disease. (F) Vascular leakage (normalized fluorescent intensity) of all brain samples were graphed against the viral RNA from each corresponding sample. Red line indicates linear regression of viral titer and vascular leakage. Pearson's correlation was performed with r and p values indicated on graph.

breaks in the CNS barrier.

Rats were infected with RVFV by aerosol (1×10^3 pfu), and then each day after infection, groups of 3 were injected with FITC-salt followed by euthanasia. Blood and brain samples were harvested and the amount of fluorescence within each sample was measured. The ratio of fluorescence in the brain to the serum was used as an indication of penetration into the tissue (Fig. 1C-E, green lines). Different regions of the brain were examined separately (olfactory bulb, cortex, cerebellum). For all 3 regions, fluorescence in the brain tissue remained at baseline levels until between 4 and 5 dpi, when there was a significant influx of fluorescein into the tissues. Viral RNA levels were measured by q-RT-PCR in the same tissue regions and the results were superimposed upon the fluorescein-salt penetration (Fig. 1C-E). It is clear that viral replication occurred in each CNS tissue prior to vascular leakage. A scatter plot showed a significant correlation between viral RNA levels and influx of fluorescein into the brain in the same piece of tissue (Fig. 1F).

To verify these results, a near-infrared (NIR) fluorescent vascular imaging agent (Superhance-680; m.w. 1540) was used in conjunction with *in vivo* imaging of live rats. A comparison of Superhance fluorescence in the brain between infected and uninfected rats can serve as an indicator of vascular leakage (Montet et al., 2006). For these experiments, a series of paired rats (one uninfected control and one rat infected with RVFV) were injected with Superhance into the tail vein. After circulation of Superhance for the indicated periods of time, each rat pair was imaged side-by-side using the IVIS-Spectrum CT (Figs. 2 and 3). Images were collected before Superhance administration (pre-injection) as an indicator of baseline autofluorescence. Since the

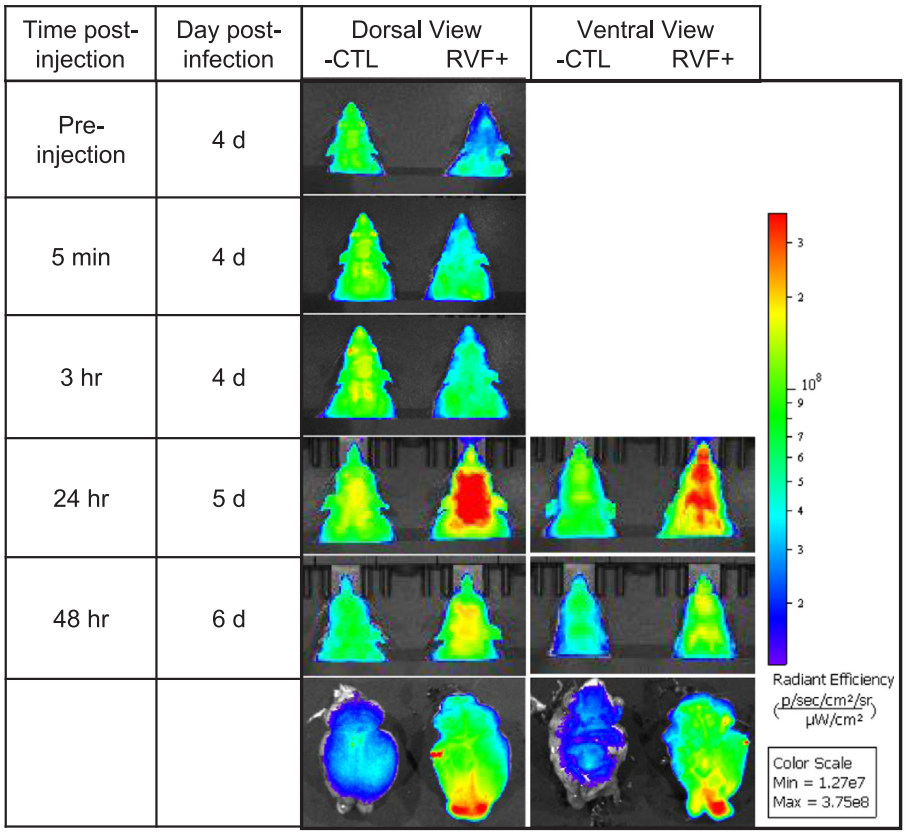

Fig. 2. *In vivo* imaging of vascular integrity in RVFV-infected rats. Lewis rats were exposed to 2×10^3 pfu of RVFV. At 4 dpi, a pair of rats was injected with Superhance 680 then imaged for fluorescent intensity at 5 min, 3 h, 24 h, and 48 h post-agent injection. This figure represents 1 pair of rats: uninfected control (-CTL; left) and an infected rat (RVF+; right) featuring both the dorsal and ventral views. After euthanasia on day 6, the brains were extracted and imaged *ex vivo* (bottom row). Radiant efficiency was normalized across samples and the scale is included.

dynamics of Superhance fluorescence in this system were unknown, a series of images were collected at 5 min (min), 3 h (h), 24 h, and 48 h after a single injection of Superhance (Fig. 2).

When Superhance was injected at 4 dpi (Fig. 2), no differences between the uninfected and infected rat were seen at 5 min and 3 h post-injection (Fig. 2). By 24 h (5 dpi), increased Superhance fluorescence was observed in the head area of the infected rat by both dorsal and ventral views. The rats were monitored for another day to determine how long the Superhance remained in circulation and detectable. Despite reduced overall signal 48 h after injection of Superhance, there was still greater fluorescence in the head region of the infected rat at 6 dpi without reinjection of Superhance. After capturing the 6 dpi image, both rats were euthanized, and the brains were excised and imaged *ex vivo*, showing that Superhance was specifically pooling in the olfactory bulb regions.

Four more pairs of rats were similarly imaged (Fig. 3A). Superhance was injected on 4 dpi or 5 dpi, and images were captured 24 h after injection of Superhance. Imaging of the brains *ex vivo* showed more Superhance fluorescence in the infected brain compared to the control. Calculating the total radiant efficiency for the whole intact heads and extracted brains, there was at least a 2-fold increased fluorescence signal in the infected animals compared to the corresponding uninfected controls (Fig. 3B). In summary, out of 5 pair of rats, vascular leakage was first detectable at 4 dpi in 1 rat, 5 dpi in 3 rats, and 6 dpi in 1 rat. The variations seen in the timing of vascular leakage correlate to the clinical window of disease, which begins on average at 5–6 dpi, but does have some variability between individual animals. Taken together, vascular permeability occurs between 4 and 5 dpi in all 3 brain regions, at the onset of clinical signs in the rats, after the virus is already replicating in the brain.

3.3. MMP-9 expression in the brain correlates with viral titer and vascular permeability

Cytokine expression in the brain is a feature of end-stage RVF encephalitis (Caroline et al., 2016; Dodd et al., 2014). Specifically MCP-1, M-CSF, Gro/KC, and IL-1β are all expressed at high levels in the brains of rats at 5–7 dpi (Caroline et al., 2016). Matrix metalloproteinase 9 (MMP-9) is an enzyme that regulates the BBB integrity by degrading and weakening the extracellular matrix and tight junctions of the vascular endothelium. Production of MMP-9 was shown to contribute to BBB opening and entry of West Nile virus (WNV) in mice (Wang et al., 2008). MMP-9 expression in the brain also contributes to the severity of Japanese encephalitis (JEV) (Shukla et al., 2012). We measured MMP-9 in the serum and the brain of RVFV-infected rats and plotted the results with viral RNA levels also measured in the corresponding samples (Fig. 4). MMP-9 levels in the brain increased with increasing levels of viral RNA, with significantly more MMP-9 in the brain at late time points (5–6 dpi). The increase in MMP-9 in the brain did not occur in the serum (Fig. 4A). The amount of MMP-9 in the brain, but not serum, correlated with viral titer in the brain. MMP-9 levels rose throughout infection, even prior to the clinical window, and were highest during the 5–6 dpi time period when vascular permeability was detectable.

4. Discussion

The integrity of the brain vasculature after arboviral infection can be a dynamic process. For WNV (family *Flaviviridae*), the mechanism by which the virus impacts BBB function appears to be multifactorial. In mice, WNV directly infects brain microvascular endothelial cells (BMECs), allowing the virus to traverse the barrier, and also increases the expression of matrix metalloproteases leading to weakening of the tight junctions within the barrier itself (Casiraghi et al., 2011; Verma et al., 2010; Wang et al., 2008). WNV also produces pro-inflammatory cytokines systemically that enhance BBB permeability in the CNS

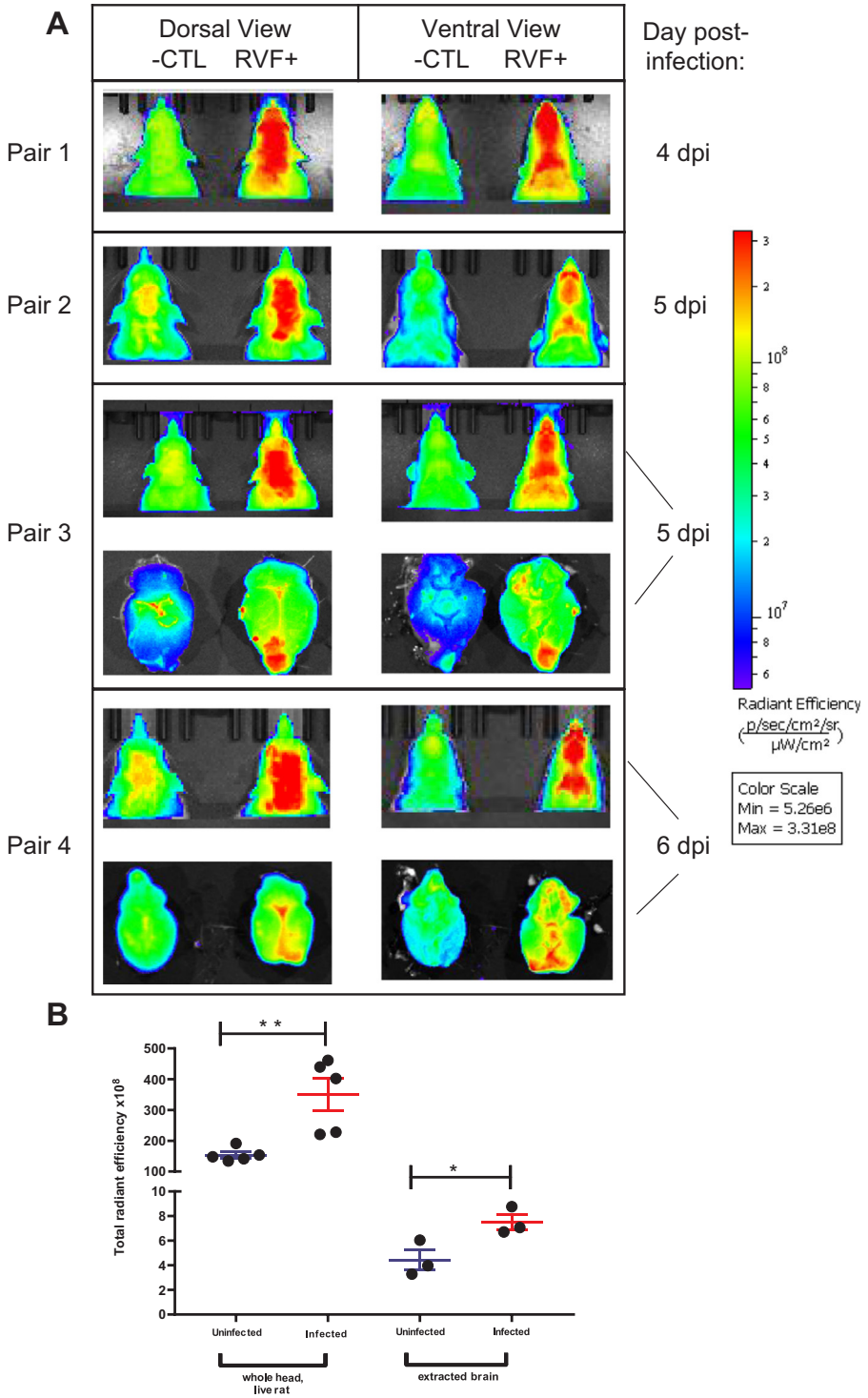

Fig. 3. Vascular integrity is compromised in lethally infected rats. (A) Four additional pairs of rats were imaged as described in Fig. 2. Each pair consists of an uninfected control (left) and infected (right) rat imaged 24 h after Superhance injection. Pairs 3 and 4 show the corresponding extracted brain. (B) Quantification of vascular leakage as determined by IVIS. Statistical significance indicated by asterisks. N = 5 for the whole-head images from live rats; n = 3 for the extracted brains.

(Shives et al., 2017). La Crosse virus (LACV) (family *Peribunyaviridae*) induces selective BBB permeability in the mouse olfactory bulb but not cortex after peripheral or systemic infection (Winkler et al., 2015). Oropouche virus (family *Peribunyaviridae*) spreads neurally from the spinal cord into the brain stem; later stages of infection result in permeability of the BBB (Santos et al., 2014). For Venezuelan equine encephalitis virus (VEEV) (family *Togaviridae*), intranasal exposure of mice results in virus entry into the brain *via* olfactory nerves, then further dissemination occurs when BBB integrity is lost first in the olfactory bulb followed by later in the cortex (Cain et al., 2017).

People can become infected with RVFV by mosquito bite or through mucosal exposure while handling dead animals (Anyangu et al., 2010; LaBeaud et al., 2015; Mohamed et al., 2010). Existing epidemiological data suggest that people living or working in close proximity to at-risk animals are more likely to develop a severe case of RVF such as hemorrhagic fever or encephalitis (Nicholas et al., 2014). This may be due to exposure route, dose, genetic polymorphisms, co-infections, or other unknown factors (Hise et al., 2015; Jansen van Vuren et al., 2015). Mice

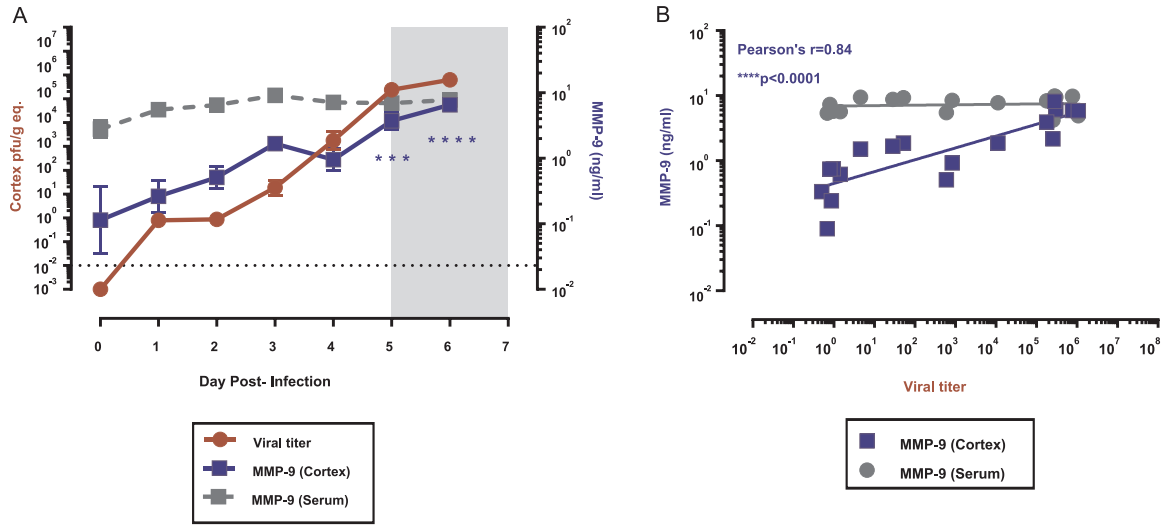

Fig. 4. Levels of MMP-9 correlate with viral titer. Lewis rats were infected with 1×10^4 pfu of RVFV by aerosol and then serially euthanized (n = 3) over a time course of six days. (A) MMP-9 levels (right y-axis) were measured in serum (gray) and brain cortex (blue) samples. Corresponding viral RNA in the brain is shown in pfu/g equivalents (red; left y-axis). The limit of detection of the PCR assay is indicted by the horizontal dotted line. The gray shaded area between 5 and 7 dpi represents the clinical window when rats display clinical signs of disease. (B) MMP-9 levels in brain samples were graphed against the viral RNA from each corresponding sample. Lines indicate linear regression of viral titer and MMP-9 levels in serum (gray) and cortex (blue). Pearson's correlation was performed for cortex samples with r and p values indicated on graph.

are a common rodent model used in RVFV studies. They primarily develop hepatic disease after subcutaneous infection, with occasional survival and progression to encephalitis (Smith et al., 2010). More consistent neurological disease can be induced in mice by intranasal infection with a virus strain lacking the non-structural NSs protein (Dodd et al., 2014). We use the rat model of encephalitis after intranasal or aerosol exposure because the animals develop reproducible disease after infection with wild-type RVFV, making them a tractable model for experimental studies.

Towards greater understanding of the neuropathogenesis of RVFV, our goal was to determine if/when CNS vascular permeability changes occur in RVFV-infected rats in relation to virus replication and other pathogenic events. The virus reaches the brain within 2 days of infection at the dose administered here, prompting the question of whether opening of the BBB is required for viral entry. Two methods of measuring vascular integrity in the brain were used: *in vivo* imaging of live animals and a more standard detection of fluorescein-salt leakage into the tissues. Virus was present and replicating in the brain several days before vascular leakage, which did not occur until 5 dpi. Rats typically succumb to RVFV infection by 7 dpi, and thus vascular permeability at 5 dpi is late in the pathogenic process. Clinical disease commences between 5 and 6 dpi, concomitant with vascular permeability. Both methods used here to measure vascular permeability do so on a macro-level, whereby we examine permeability in the head of a live animal, a whole extracted brain, or an extracted brain region. However, we cannot rule out the possibility that temporary micro-level vascular opening occurs earlier in infection to allow virus to enter. Histology studies are currently underway to address this. Despite this caveat, the vascular permeability that we observed here occurred late during the course of infection, well after virus was present and replicating in the CNS.

We found that both vascular leakage and MMP-9 levels in brain tissue correlate with virus titer. The data shown here suggest that RVF enters the brain without requiring global disruption of the BBB, most likely achieved either directly *via* the olfactory epithelium or through the lymphatic system in an as-yet undefined mechanism. The levels of MMP-9 increase in correlation with increasing virus titers. At 5 dpi, global vascular leakage is detected, along with high levels of virus, MMP-9 and other cytokines (Caroline et al., 2016). This work contributes to our understanding of the course of encephalitic RVF in the rat model and suggests that prevention of vascular leakage late in infection may be an important component for prevention of lethal neurological disease in rats.

Acknowledgements

The authors recognize Katherine J. O'Malley and Dr. Douglas S. Reed for performing the aerosol exposures. We also thank Dr. Christina Gardner for assistance with *in vivo* imaging.

Funding information

This work was supported in part by U.S. National Institutes of Health award 1R21NS088326-01A1 to ALH and U.S. Department of Defense (DoD) Award HDTRA1-11-16 BRCWMC-BAA to WBK and ALH. The funders had no role in study design, data collection and interpretation, or the decision to submit the work for publication.

Author contributions

W.B.K. and A.L.H conceived and designed the experiments; A.W.W., M.R.K., J.R.A., D.S.R., and A.L.H. performed experimental work; A.L.H. analyzed and interpreted the data and wrote the manuscript.

References

Al-Hazmi, M., Ayoola, E.A., Abdurahman, M., Banzal, S., Ashraf, J., El-Bushra, A., Hazmi, A., Abdullah, M., Abbo, H., Elamin, A., Al-Sammani el, T., Gadour, M., Menon, C., Hamza, M., Rahim, I., Hafez, M., Jambavalikar, M., Arishi, H., Aqeel, A., 2003. Epidemic Rift Valley fever in Saudi Arabia: a clinical study of severe illness in humans. Clin. Infect. Dis. 36, 245–252.

Anyangu, A.S., Gould, L.H., Sharif, S.K., Nguku, P.M., Omolo, J.O., Mutonga, D., Rao, C.Y., Lederman, E.R., Schnabel, D., Paweska, J.T., Katz, M., Hightower, A., Njenga, M.K., Feikin, D.R., Breiman, R.F., 2010. Risk factors for severe Rift Valley fever infection in Kenya, 2007. Am. J. Trop. Med. Hyg. 83, 14–21.

Bales, J.M., Powell, D.S., Bethel, L.M., Reed, D.S., Hartman, A.L., 2012. Choice of inbred rat strain impacts lethality and disease course after respiratory infection with Rift Valley Fever Virus. Front. Cell. Infect. Microbiol. 2, 105.

Bird, B.H., Reynes, J.M., Nichol, S.T., 2012. Rift Valley Fever. In: Magill, A.J., Strickland, G.T., Maguire, J.H., Ryan, E.T., Solomon, T. (Eds.), Hunter's Tropical Medicine and Emerging Infectious Disease, 9th ed. Elsevier Health Sciences, China, pp. 340–343.

Boushab, B.M., Fall-Malick, F.Z., Baba, S.E.W.O., Salem, M.L.O., Belizaire, M.R.D., Ledib, H., Ahmed, M.M.O.B., Basco, L.K., Ba, H., 2016. Severe human illness caused by rift valley fever virus in Mauritania, 2015. Open Forum Infect. Dis. 3.

Cain, M.D., Salimi, H., Gong, Y., Yang, L., Hamilton, S.L., Heffernan, J.R., Hou, J., Miller, M.J., Klein, R.S., 2017. Virus entry and replication in the brain precedes blood-brain barrier disruption during intranasal alphavirus infection. J. Neuroimmunol. 308, 118–130.

Caroline, A.L., Kujawa, M.R., Oury, T.D., Reed, D.S., Hartman, A.L., 2016. Inflammatory biomarkers associated with lethal Rift Valley fever encephalitis in the Lewis Rat model. Front. Microbiol. 6, 1509.

Casiraghi, C., Dorovini-Zis, K., Horwitz, M.S., 2011. Epstein-Barr virus infection of human brain microvessel endothelial cells: a novel role in multiple sclerosis. J. Neuroimmunol. 230, 173–177.

Dodd, K.A., McElroy, A.K., Jones, T.L., Zaki, S.R., Nichol, S.T., Spiropoulou, C.F., 2014. Rift valley Fever virus encephalitis is associated with an ineffective systemic immune response and activated T cell infiltration into the CNS in an immunocompetent mouse model. PLoS Negl. Trop. Dis. 8, e2874.

Gowen, B.B., Bailey, K.W., Scharton, D., Vest, Z., Westover, J.B., Skirpstunas, R., Ikegami, T., 2013. Post-exposure vaccination with MP-12 lacking NSs protects mice against lethal Rift Valley fever virus challenge. Antivir. Res. 98, 135–143.

Hartman, A.L., Powell, D.S., Bethel, L.M., Caroline, A.L., Schmid, R.J., Oury, T., Reed, D.S., 2014. Aerosolized rift valley fever virus causes fatal encephalitis in african green monkeys and common marmosets. J. Virol. 88, 2235–2245.

Hise, A.G., Traylor, Z., Hall, N.B., Sutherland, L.J., Dahir, S., Ermler, M.E., Muiruri, S., Muchiri, E.M., Kazura, J.W., LaBeaud, A.D., King, C.H., Stein, C.M., 2015. Association of symptoms and severity of rift valley fever with genetic polymorphisms in human innate immune pathways. PLoS Negl. Trop. Dis. 9, e0003584.

Jansen van Vuren, P., Shalekoff, S., Grobbelaar, A.A., Archer, B.N., Thomas, J., Tiemessen, C.T., Paweska, J.T., 2015. Serum levels of inflammatory cytokines in Rift Valley fever patients are indicative of severe disease. Virol. J. 12, 159.

LaBeaud, A.D., Pfeil, S., Muiruri, S., Dahir, S., Sutherland, L.J., Traylor, Z., Gildengorin, G., Muchiri, E.M., Morrill, J., Peters, C.J., Hise, A.G., Kazura, J.W., King, C.H., 2015. Factors associated with severe human Rift Valley fever in Sangailu, Garissa County, Kenya. PLoS Negl. Trop. Dis. 9, e0003548.

Louveau, A., Smirnov, I., Keyes, T.J., Eccles, J.D., Rouhani, S.J., Peske, J.D., Derecki, N.C., Castle, D., Mandell, J.W., Lee, K.S., Harris, T.H., Kipnis, J., 2015. Structural and functional features of central nervous system lymphatic vessels. Nature 523, 337–341.

Madani, T.A., Al-Mazrou, Y.Y., Al-Jeffri, M.H., Mishkhas, A.A., Al-Rabeah, A.M., Turkistani, A.M., Al-Sayed, M.O., Abodahish, A.A., Khan, A.S., Ksiazek, T.G., Shobokshi, O., 2003. Rift Valley fever epidemic in Saudi Arabia: epidemiological, clinical, and laboratory characteristics. Clin. Infect. Dis. 37, 1084–1092.

McGavern, D.B., Kang, S.S., 2011. Illuminating viral infections in the nervous system. Nat. Rev. Immunol. 318–329.

Meegan, J.M., 1979. The Rift Valley fever epizootic in Egypt 1977-78. 1. Description of the epizootic and virological studies. Trans. R. Soc. Trop. Med. Hyg. 73, 618–623.

Mohamed, M., Mosha, F., Mghamba, J., Zaki, S.R., Shieh, W.J., Paweska, J., Omulo, S., Gikundi, S., Mmbuji, P., Bloland, P., Zeidner, N., Kalinga, R., Breiman, R.F., Njenga, M.K., 2010. Epidemiologic and clinical aspects of a Rift Valley fever outbreak in humans in Tanzania, 2007. Am. J. Trop. Med. Hyg. 83, 22–27.

Montet, X., Rajopadhye, M., Weissleder, R., 2006. An albumin-activated Far-Red fluorochrome for *in vivo* imaging. ChemMedChem 1, 66–69.

Mutua, E.N., Bukachi, S.A., Bett, B.K., Estambale, B.A., Nyamongo, I.K., 2017. "We do not bury dead livestock like human beings": community behaviors and risk of Rift Valley Fever virus infection in Baringo County, Kenya. PLoS Negl. Trop. Dis. 11, e0005582.

Nicholas, D.E., Jacobsen, K.H., Waters, N.M., 2014. Risk factors associated with human Rift Valley fever infection: systematic review and meta-analysis. Trop. Med. Int. Health 19, 1420–1429.

Rakotoarivelo, R.A., Andrianasolo, R., Razafimahefa, S.H., Randremandranto Razafimbelo, N.S., Randria, M.J.D., 2011. Les formes graves de la fièvre de la vallée de Rift pendant l'épidémie à Madagascar. Méd. Mal. Infect. 41, 318–321.

Reed, C., Lin, K., Wilhelmsen, C., Friedrich, B., Nalca, A., Keeney, A., Donnelly, G., Shamblin, J., Hensley, L.E., Olinger, G., Smith, D.R., 2013. Aerosol exposure to Rift Valley fever virus causes earlier and more severe neuropathology in the murine model, which has important implications for therapeutic development. PLoS Negl. Trop. Dis. 7, e2156.

Santos, R., Bueno-Júnior, L., Ruggiero, R., Almeida, M., Silva, M., Paula, F., Correa, V., Arruda, E., 2014. Spread of Oropouche Virus into the central nervous system in mouse. Viruses 6, 3827–3836.

Schafer, A., Brooke, C.B., Whitmore, A.C., Johnston, R.E., 2011. The role of the blood-brain barrier during Venezuelan equine encephalitis virus infection. J. Virol. 85, 10682–10690.

Scharton, D., Bailey, K.W., Vest, Z., Westover, J.B., Kumaki, Y., Van Wettere, A., Furuta, Y., Gowen, B.B., 2014. Favipiravir (T-705) protects against peracute Rift Valley fever virus infection and reduces delayed-onset neurologic disease observed with ribavirin treatment. Antivir. Res. 104, 84–92.

Shives, K.D., Tyler, K.L., Beckham, J.D., 2017. Molecular mechanisms of neuroinflammation and injury during acute viral encephalitis. J. Neuroimmunol. 308, 102–111.

Shukla, V., Kumar Shakya, A., Dhole, T.N., Misra, U.K., 2012. Upregulated expression of matrix metalloproteinases and tissue inhibitors of matrix metalloproteinases in BALB/c mouse brain challenged with Japanese encephalitis virus. Neuroimmunomodulation 19, 241–254.

Smith, D.R., Bird, B.H., Lewis, B., Johnston, S.C., McCarthy, S., Keeney, A., Botto, M., Donnelly, G., Shamblin, J., Albarino, C.G., Nichol, S.T., Hensley, L.E., 2012. Development of a novel nonhuman primate model for Rift Valley fever. J. Virol. 86, 2109–2120.

Smith, D.R., Steele, K.E., Shamblin, J., Honko, A., Johnson, J., Reed, C., Kennedy, M., Chapman, J.L., Hensley, L.E., 2010. The pathogenesis of Rift Valley fever virus in the mouse model. Virology 407, 256–267.

Verma, S., Kumar, M., Gurjav, U., Lum, S., Nerurkar, V.R., 2010. Reversal of West Nile virus-induced blood–brain barrier disruption and tight junction proteins degradation by matrix metalloproteinases inhibitor. Virology 397, 130–138.

Wang, P., Dai, J., Bai, F., Kong, K.F., Wong, S.J., Montgomery, R.R., Madri, J.A., Fikrig, E., 2008. Matrix metalloproteinase 9 facilitates west nile virus entry into the brain. J. Virol. 82, 8978–8985.

Winkler, C.W., Race, B., Phillips, K., Peterson, K.E., 2015. Capillaries in the olfactory bulb but not the cortex are highly susceptible to virus-induced vascular leak and promote viral neuroinvasion. Acta Neuropathol. 130, 233–245.